Model-Based Filters for 3-D Positioning of Marine Mammals Using AHRS- and GPS-Equipped UAVs

TIAGO GASPAR, Member, IEEE
PAULO OLIVEIRA, Senior Member, IEEE
CARLOS SILVESTRE, Member, IEEE
Institute for Systems and Robotics
Lisbon, Portugal

This work tackles the problem of estimating the position of a marine mammal moving at the ocean surface by using an unmanned aerial vehicle equipped with a camera, a GPS receiver, and an attitude and heading reference system. Two Kalman filters—inserted on a multiple-model adaptive estimation framework—which use an unstable model for the target depending on an unknown parameter that must be identified (its angular speed) are proposed and compared with an extended Kalman filter.

Manuscript received October 7, 2014; revised March 20, 2015; released for publication May 31, 2015.

DOI. No. 10.1109/TAES.2015.140748.

Refereeing of this contribution was handled by L. Mihaylova.

This work was partially supported by the Fundação para a Ciência e a Tecnologia (FCT) through Institute for Systems and Robotics (ISR), under Associated Laboratory for Robotics and Engineering Systems (LARSyS) (UID/EEA/50009/2013) and through Institute for Mechanical Engineering (IDMEC), under Associated Laboratory for Energy, Transports and Aeronautics (LAETA) (UID/EMS/50022/2013) projects, and by projects MYRG2015-00126-FST and MYRG2015-00127-FST of the University of Macau. The work of Tiago Gaspar was supported by PhD Student Scholarship SFRH/BD/46860/2008, from FCT.

Authors' addresses: The authors are with the Institute for Systems and Robotics, Laboratory of Robotics and Engineering Systems, Av. Rovisco Pais, 1, 1049-001 Lisboa, Portugal.

T. Gaspar is with the Instituto Superior Técnico, Universidade de Lisboa, Av. Rovisco Pais, 1, 1049-001 Lisboa, Portugal, E-mail: tgaspar@isr.ist.utl.pt; P. Oliveira, is with LAETA and the Department of Mechanical Engineering, Instituto Superior Técnico, Universidade de Lisboa, Av. Robisco Pais, 1, 1049-001 Lisboa, Portugal, E-mail: p.oliveira@dem.tecnico.ulisboa.pt; C. Silvestre is with the Department of Electrical and Computer Engineering of the Faculty of Science and Technology of the University of Macau, E11, Avenida da Universidade, Taipa, Macau, China, on leave from Instituto Superior Tcnico, Universidade de Lisboa, Lisboa, Portugal, E-mail: csilvestre@umac.mo.

0018-9251/15/$26.00

I. INTRODUCTION

In the last decades there has seen a significant increase in the use of systems such as acoustic telemetry [1], or pop-up satellite archival tags [2], to study, for instance, the daily motion patterns and behavior of marine animals [1, 3] and migration patterns in marine protected areas [1]. More recently, the developments made in the capabilities of unmanned aerial vehicles (UAVs) [4] have transformed them into useful tools for ocean-surface data acquisition. However, most of these vehicles have been designed to conduct simple survey missions that in general do not require close interaction between the operator and the environment. Thus it is by now felt that the effective use of UAVs in demanding marine-science applications must be clearly demonstrated, namely by evaluating UAV-based systems in terms of their performance and adaptability to different missions scenarios.

One of the marine-science areas that can profit from the use of UAVs is positioning and tracking of marine mammals [5]. Other applications are also foreseen that use autonomous vehicles as useful tools to help marine scientists, namely in measuring the sea surface temperature and in directing research vessels to new areas of interest, leading to a more efficient use of the ship time.

In this work, the problem of estimating the position of a marine mammal moving at the ocean surface is addressed. With this purpose, a UAV instrumented with a GPS receiver, an attitude and heading reference system (AHRS), and an image-acquisition module—which consists of a digital video camera mounted on a pan-tilt unit—is considered. The intrinsically nonlinear problem that results is cast into a linear form by using the measurements provided by the camera in a nonstandard manner. Under this scope, two linear Kalman filters (KFs) are proposed that estimate the state of the target (composed of its 3-D position and velocity) by merging the camera measurements with the UAV position and attitude measurements provided by the GPS receiver and AHRS, respectively: one, time invariant, that estimates only the state of the target, and the other, time varying, that combines estimates of the state of the target with estimates of the state of the UAV to improve the overall performance. These filters are included in a multiple-model adaptive estimation (MMAE) framework; see [6, 7] for details about this type of approach, which copes with the unknown nature of one of the parameters of the model considered for the target (its angular speed). A set of simulations carried out under realistic noise conditions is provided, and occlusions, which occur when the marine mammal dives, are also simulated. For comparison purposes, results are also presented that are obtained with an extended Kalman filter (EKF), designed for the nonlinear system that results from augmenting the state of the target with its angular speed.

This work is an evolution of that proposed in [8]. The main differences are 1) a new structure for the time-invariant and time-varying filters, which were modified to accommodate observations that are obtained according to different transformations of the sensor measurements; 2) a new (extended) Kalman filter; and 3) new simulation results that compare the performance of the new filters with that of the EKF and that show that the true target model is identified correctly.

A. Related Work

The use of UAVs for target tracking and positioning, in conjunction with vision-based systems, has received a lot of attention from the scientific community; see the examples in [9–18]. In addition to all the challenges associated with the typical vision-based positioning and tracking systems, in which the cameras are static, using moving cameras—in this case installed on a UAV—poses additional difficulties. Given the complexity of the problem, a number of different approaches have been pursued. Some of the existing methods try to solve the problem by imposing constraints on the motion of the target or of the UAV. The results presented in [17, 18], for instance, are only possible if the target moves with constant velocity, and the ones presented in [19] require the design of a path-planning strategy for the UAV. Both requirements are very restrictive and difficult to meet in real scenarios. In [9], a UAV path-planning strategy is also used, but in this case with the goal of minimizing the influence of sunlight reflections in the identification of objects moving at the water surface, not with the goal of keeping the UAV with a given position and attitude with respect to the target.

One of the difficulties that arise in visual tracking using UAVs consists in estimating the altitude of the UAV (and consequently the altitude of the cameras). Some of the existing approaches—see for instance [15, 20]—require the existence of highly accurate geo-referenced terrain databases, such as the Geographical Information System, and others (see [21]) use other types of sensors, like laser scanners. However, accurate terrain databases are not always available, and such sensors are heavy and a power burden. In our setup, the need for this type of approach is significantly reduced, as the target is known to move at the ocean surface, which can be accurately approximated by a plane.

Another typical challenge in target tracking is the occlusion of the moving object. In [12], for instance, the authors use the redundancy brought into play by the use of multiple UAVs to improve the target position estimates and to guarantee a continuous monitoring of the moving object, even when individual vehicles experience failures. Such an approach is particularly appropriate for environments with many obstacles, which is not the case when the target moves on the ocean. In this situation, occlusions result mostly from dives of the marine mammal, and we deal with them by feeding the proposed estimator with an appropriate model for the target that allows a good prediction of its position while it is submerged.

The specific topic of using one camera installed on a UAV to monitor marine animals has been addressed before—see, for instance, [13]. However, such research is mostly focused on the study of an image-processing method to identify the target (in that case a whale moving in an ocean environment), whereas the main goal of our work is to provide new filtering strategies that lead to improvements in the accuracy of the final estimates for the target position.

Different frameworks, in which a single UAV is used to track several targets simultaneously, have also been studied in the literature. This is the case in [11], where there are no requirements regarding any particular path-planning strategy or the existence of a geo-referenced terrain database. On the other hand, such work uses feature points extracted from the ground surrounding the targets to calculate the height of the vehicle, similar to what happens in [14], where feature points are used to estimate the pose of the UAV. The use of this type of method is difficult, if not impossible, in ocean environments, which are very dynamic and usually featureless.

The problems addressed in [10, 16] are close to the one addressed here. In the first case, the authors propose a nonlinear adaptive observer that provides estimates for the position of the target. This approach differs from our formulation, which casts the estimation problem into a linear form. The target position estimates provided by the second method are biased, as the attitude of the aircraft is not measured directly (it is inferred using a single-antenna GPS-based attitude-determination method). This is not the case for our approach, which makes use of the measurements provided by the AHRS to circumvent this disadvantage.

B. Outline of the Paper

This paper is organized as follows. The problem addressed in this work is described in Section II, as are the models considered for the target, UAV, and sensors. The filters proposed for the positioning problem at hand are addressed in Section III, and in Section IV simulation results are presented and discussed. Finally, some concluding remarks are given in Section V.

II. PROBLEM STATEMENT

Consider a UAV instrumented with an AHRS that provides estimates of the orientation ${}^{I}\mathbf{R}_p(t) \in SO(3)$ of a body-fixed frame $\{P\}$, attached to the UAV, with respect to an inertial reference frame $\{I\}$, over time t—${}^{I}\mathbf{R}_p(t)$ is the rotation matrix that rotates the coordinates of points from frame $\{P\}$ to frame $\{I\}$. A GPS receiver installed aboard the UAV provides estimates of the position ${}^{I}\mathbf{X}_p(t) \in \mathbb{R}^3$ of the origin of $\{P\}$ expressed in the inertial frame $\{I\}$. Without loss of generality, the inertial reference frame is considered to have its origin in the vicinity of the mission scenario and at the sea surface, with the z-axis orthogonal to it and pointing upward (see Fig. 1). The UAV is also instrumented with an image-acquisition module, which

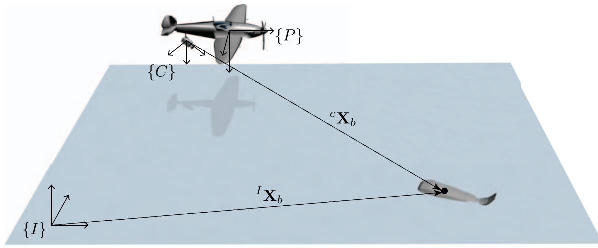

Fig. 1. Example of mission scenario for tracking and positioning of marine mammals.

consists of a digital video camera mounted on a pan-tilt unit. The position ${}^{p}\mathbf{X}_c \in \mathbb{R}^3$ of the origin of a body-fixed frame $\{C\}$ attached to the camera, expressed in the aircraft frame $\{P\}$ and the orientation ${}^{p}\mathbf{R}_c \in SO(3)$ of $\{C\}$ with respect to $\{P\}$, is known—${}^{p}\mathbf{R}_c$ is the rotation matrix that rotates the coordinates of points from frame $\{C\}$ to frame $\{P\}$. The origin of $\{C\}$ is at the camera optical center, and its z-axis is aligned with the camera optical axis.

Moreover, consider a marine mammal moving at the sea surface and denote the inertial coordinates of its position by ${}^{I}\mathbf{X}_b(t) \in \mathbb{R}^3$. According to the described setup, the position of the target in the inertial reference frame is given by the vector ${}^{I}\mathbf{X}_b(t) = [\,{}^{I}x_b(t) \quad {}^{I}y_b(t)\ 0\,]^{\mathrm{T}}$.

The problem addressed in this article is that of tracking the marine mammal and obtaining estimates $[\,{}^{I}\hat{x}_b(t) \quad {}^{I}\hat{y}_b(t)\,]^{\mathrm{T}}$ for its position, using measurements provided by the GPS receiver, the AHRS, and the image-acquisition module. These measurements are considered to be corrupted by white Gaussian noise.

A. Marine-Mammal Model

State-space models have been used in the characterization of the movement of several animals, as reported in [22]. In the following, the dynamical model chosen for the marine mammal is described. Given the trajectories expected for this type of target—which, as stated before, is assumed to lie in a plane coincident with the sea surface—the 2D Horizontal Constant-Turn Model With Known Turn Rate, as presented in [23], is selected. This model assumes that the target moves with constant speed and constant angular (turn) rate ω, here also referred to as angular speed (norm of the angular velocity vector). Assuming that ω is known, a four-dimensional state vector $\mathbf{x}_b(t) = [\,{}^{I}x_b(t) \quad {}^{I}\dot{x}_b(t) \quad {}^{I}y_b(t) \quad {}^{I}\dot{y}_b(t)\,]^{\mathrm{T}}$ results, where $[\,{}^{I}x_b(t) \quad {}^{I}y_b(t)\,]^{\mathrm{T}}$ and $[\,{}^{I}\dot{x}_b(t) \quad {}^{I}\dot{y}_b(t)\,]^{\mathrm{T}}$ are, respectively, the position and velocity of the target expressed in inertial coordinates. Let $\mathbf{x}_b(t_k)$ denote the value taken by the state $\mathbf{x}_b(t)$ of the target at time instant $t_k = kT$, $k \in \mathbb{N}$, where $T > 0$ is the sampling interval. In this case, the target state dynamics assumes the following linear parametrically varying form:

$$\begin{aligned}\mathbf{x}_b(t_k) &= \mathbf{F}_b(\omega)\,\mathbf{x}_b(t_{k-1}) + \mathbf{w}_b(t_{k-1}) \\ &= \begin{bmatrix} 1 & \dfrac{\sin(\omega T)}{\omega} & 0 & -\dfrac{1-\cos(\omega T)}{\omega} \\ 0 & \cos(\omega T) & 0 & -\sin(\omega T) \\ 0 & \dfrac{1-\cos(\omega T)}{\omega} & 1 & \dfrac{\sin(\omega T)}{\omega} \\ 0 & \sin(\omega T) & 0 & \cos(\omega T) \end{bmatrix} \\ &\quad \times \mathbf{x}_b(t_{k-1}) + \mathbf{w}_b(t_{k-1}). \end{aligned} \tag{1}$$

The process noise $\mathbf{w}_b(t_k) \in \mathbb{R}^4$ is assumed to be Gaussian and to have zero mean, with the covariance matrix

$$\mathbf{Q}_b(\omega) = S_{w_b} \begin{bmatrix} \dfrac{2(\omega T - \sin(\omega T))}{\omega^3} & \dfrac{1-\cos(\omega T)}{\omega^2} & 0 & \dfrac{\omega T - \sin(\omega T)}{\omega^2} \\ \dfrac{1-\cos(\omega T)}{\omega^2} & T & -\dfrac{\omega T - \sin(\omega T)}{\omega^2} & 0 \\ 0 & -\dfrac{\omega T - \sin(\omega T)}{\omega^2} & \dfrac{2(\omega T - \sin(\omega T))}{\omega^3} & \dfrac{1-\cos(\omega T)}{\omega^2} \\ \dfrac{\omega T - \sin(\omega T)}{\omega^2} & 0 & \dfrac{1-\cos(\omega T)}{\omega^2} & T \end{bmatrix}, \tag{2}$$

where S_{w_b} corresponds to the power spectral density of the continuous-time process noises that affect the two components of the velocity of the target. Note that neither $\mathbf{F}_b(\omega)$ nor $\mathbf{Q}_b(\omega)$ is defined for $\omega = 0$. When this is the case, the limit of these two matrices as ω approaches 0 is used. More details about this model can be found in [23].

Note that the state dynamics and the process-noise covariance matrix depend explicitly on the target angular speed, whose actual value is not known. A solution that copes with this problem is proposed in Section III.

B. UAV Model

In order to keep the positioning system proposed in this article as general as possible, the dynamics of the UAV are modeled as a double integrator. A more complex model could have been used, but this approach leads to a general solution that suits systems with different types of aircrafts.

Let the state of the UAV be given by the vector $\mathbf{x}_p(t) = [\,{}^{I}x_p\ {}^{I}\dot{x}_p\ {}^{I}\ddot{x}_p\ {}^{I}y_p\ {}^{I}\dot{y}_p\ {}^{I}\ddot{y}_p\ {}^{I}z_p\ {}^{I}\dot{z}_p\ {}^{I}\ddot{z}_p\,]^{\mathrm{T}}$, where $[\,{}^{I}x_p\ {}^{I}y_p\ {}^{I}z_p\,]^{\mathrm{T}}$, $[\,{}^{I}\dot{x}_p\ {}^{I}\dot{y}_p\ {}^{I}\dot{z}_p\,]^{\mathrm{T}}$, and $[\,{}^{I}\ddot{x}_p\ {}^{I}\ddot{y}_p\ {}^{I}\ddot{z}_p\,]^{\mathrm{T}}$

denote, respectively, the UAV 3-D position, velocity, and acceleration, expressed in inertial coordinates. The dependence of the scalar quantities on time t was omitted for simplicity of presentation. The process noise that affects the three components of the acceleration of the UAV is assumed to be Gaussian and zero-mean, with the power spectral density matrix diag$[S_{w_p}\ S_{w_p}\ S_{w_p}]$, where $S_{w_p} \in \mathbb{R}$ is the power spectral density associated with each individual process-noise component. Under these assumptions, the motion of the UAV can be described by the discrete-time state equation

$$\mathbf{x}_p(t_k) = \mathbf{F}_p \mathbf{x}_p(t_{k-1}) + \mathbf{w}_p(t_{k-1}),$$

where $t_k = kT$, $t_{k-1} = (k-1)T$, $k \in \mathbb{N}$, and $T > 0$ is the sampling interval (see [24]). In this equation, $\mathbf{F}_p = \text{diag}[\,\mathbf{F}\ \mathbf{F}\ \mathbf{F}\,]$, and the value of the discrete-time process noise $\mathbf{w}_p(t_k)$ is associated with the covariance matrix $\mathbf{Q}_p = \text{diag}[\,S_{w_p}\mathbf{Q}\ S_{w_p}\mathbf{Q}\ S_{w_p}\mathbf{Q}\,]$, with

$$\mathbf{F} = \begin{bmatrix} 1 & T & T^2/2 \\ 0 & 1 & T \\ 0 & 0 & 1 \end{bmatrix}$$

and

$$\mathbf{Q} = \begin{bmatrix} T^5/20 & T^4/8 & T^3/6 \\ T^4/8 & T^3/3 & T^2/2 \\ T^3/6 & T^2/2 & T \end{bmatrix}.$$

The notation diag$[\cdot]$ is used to denote a diagonal matrix whose entries are the ones indicated between brackets.

C. Measurement Model

The UAV is instrumented with a GPS receiver and an AHRS, which provide measurements of its position and attitude with respect to $\{I\}$, and with an image-acquisition module that acquires images of a marine mammal moving at the sea surface. The measurements provided by these sensors are described in this section.

The data obtained from the GPS and AHRS correspond to direct measurements of the position ${}^I\mathbf{X}_p$ and orientation ${}^I\mathbf{R}_p$ of the UAV with respect to the inertial reference frame. Measurements provided by the image-acquisition module are more intricate. Given the high complexity of camera optical systems and the consequent high number of parameters required to model the whole image-acquisition process, it is common to use simplified camera models. In this work, the pinhole model is considered (see [25] for details).

Let us assume that the centroid of the image of the marine mammal is the projection of the point used to define the position ${}^I\mathbf{X}_b$ of the target in the inertial reference frame, and let the coordinates of this point in the image frame be denoted by (u, v). Then, according to the pinhole model, these coordinates can be written in the form

$$u = \frac{p_{11}{}^I x_b + p_{12}{}^I y_b + p_{14}}{p_{31}{}^I x_b + p_{32}{}^I y_b + p_{34}},$$
$$v = \frac{p_{21}{}^I x_b + p_{22}{}^I y_b + p_{24}}{p_{31}{}^I x_b + p_{32}{}^I y_b + p_{34}}, \tag{3}$$

where p_{ij} is the element of the projection matrix in the ith line and jth column. As can be seen, these measurements are a nonlinear function of the position ${}^I\mathbf{X}_b$ of the target. The absence of a z-component in this expression is due to the fact that, according to the setup described in the beginning of this section, the 3-D position of the target is given by ${}^I\mathbf{X}_b = [\,{}^I x_b\ {}^I y_b\ 0\,]^{\mathrm{T}}$.

The marine mammal can be segmented by resorting, for instance, to active contours (see [26, 27]). Moreover, the coordinates in the image of the point that defines the target position, in this case the center of its boundary, can be easily computed as the average of the coordinates of the points that belong to the estimated contour.

III. FILTER DESIGNS

In this section, several estimation strategies that solve the positioning problem at hand are presented: two KFs with different structures and an EKF. The two KFs are here called isolated and joint, depending on the use or not of estimates of the state of the UAV to help in the estimation of the state of the target. The linear KFs are proposed under the MMAE framework to deal with the unknown nature of the target angular speed. The Baram proximity measure (BPM) [28] is used to provide some insight into how to choose the nominal angular-speed values for each underlying KF model.

A. Isolated KF

When the pinhole model is considered, the relation between the coordinates ${}^I\mathbf{X}_b$ of the point that represents the target and the coordinates (u, v) of the projection of that point onto the image frame is nonlinear; see (3). A filter that combined these expressions in their present form with the model in (1) to obtain estimates for the marine mammal's position would hardly have any stability and performance guarantees. An example of such a strategy is provided in Section III-D, where an EKF is presented for comparison purposes. Here, a different approach is proposed, which consists in rewriting (3) as a linear function of the state of the system.

Let $\mathbf{A}_c$ denote the 3×3 matrix with the intrinsic parameters of the camera, and $[\,{}^c\mathbf{R}_I \,|\, {}^c\mathbf{X}_I\,]$ its 3×4 external parameters matrix, where ${}^c\mathbf{R}_I$ and ${}^c\mathbf{X}_I$ are, respectively, the rotation matrix that rotates points from $\{I\}$ to $\{C\}$ and the origin of $\{I\}$ expressed in $\{C\}$. Using this notation, the projection matrix of the camera at each time instant (note that the dependence on time is omitted here to keep the notation simple) has the form

$\mathbf{A}_c[{}^c\mathbf{R}_I \,|\, {}^c\mathbf{X}_I\,]$. Thus, u and v in (3) can be rewritten as

$$u = \frac{\mathbf{e}_1^{\mathrm{T}}\mathbf{A}_c\left({}^c\mathbf{R}_I{}^I\mathbf{X}_b + {}^c\mathbf{X}_I\right)}{\mathbf{e}_3^{\mathrm{T}}\mathbf{A}_c\left({}^c\mathbf{R}_I{}^I\mathbf{X}_b + {}^c\mathbf{X}_I\right)}, \quad v = \frac{\mathbf{e}_2^{\mathrm{T}}\mathbf{A}_c\left({}^c\mathbf{R}_I{}^I\mathbf{X}_b + {}^c\mathbf{X}_I\right)}{\mathbf{e}_3^{\mathrm{T}}\mathbf{A}_c\left({}^c\mathbf{R}_I{}^I\mathbf{X}_b + {}^c\mathbf{X}_I\right)},$$

where $\mathbf{e}_i$, $i = 1, 2, 3$, is used to denote the ith vector of the canonical basis of $\mathbb{R}^3$. If $\mathbf{m} = [\,u \;\; v \;\; 1\,]^{\mathrm{T}}$ is used to denote the homogeneous coordinates associated with (u, v) [25], then according to the pinhole model and using the properties of rigid-body transformations (see details in [29]), it is possible to rewrite these expressions, and therefore (3), in the form

$$\begin{aligned}\lambda\mathbf{m} &= \mathbf{A}_c\left({}^c\mathbf{R}_I{}^I\mathbf{X}_b + {}^c\mathbf{X}_I\right)\\ &= \mathbf{A}_c{}^p\mathbf{R}_c^{\mathrm{T}}\left[{}^I\mathbf{R}_p^{\mathrm{T}}\left({}^I\mathbf{X}_b - {}^I\mathbf{X}_p\right) - {}^p\mathbf{X}_c\right],\end{aligned} \tag{4}$$

where $\lambda = \mathbf{e}_3^{\mathrm{T}}\mathbf{A}_c({}^c\mathbf{R}_I{}^I\mathbf{X}_b + {}^c\mathbf{X}_I)$ is a scaling factor related to the distance from the target to the camera. Apart from λ and ${}^I\mathbf{X}_b$, all the other quantities in this equation are either known ($\mathbf{A}_c$, ${}^p\mathbf{R}_c$, and ${}^p\mathbf{X}_c$ are calibrated) or measured ($\mathbf{m}$, ${}^I\mathbf{R}_p$, and ${}^I\mathbf{X}_p$). Given the constraint ${}^Iz_b = 0$ on the third component of ${}^I\mathbf{X}_b$, (4) is a linear system with three equations and three unknowns (λ, ${}^Ix_b$, and ${}^Iy_b$). By rearranging the terms in (4), we have

$$\underbrace{\left[-\mathbf{A}_c{}^p\mathbf{R}_c^{\mathrm{T}}{}^I\mathbf{R}_p^{\mathrm{T}}\mathbf{M} \quad \mathbf{m}\right]}_{\mathbf{Q}_I}\begin{bmatrix}{}^Ix_b\\ {}^Iy_b\\ \lambda\end{bmatrix} = \underbrace{-\mathbf{A}_c{}^p\mathbf{R}_c^{\mathrm{T}}\left({}^I\mathbf{R}_p^{\mathrm{T}}{}^I\mathbf{X}_p - {}^p\mathbf{X}_c\right)}_{\mathbf{b}_I},$$

where $\mathbf{Q}_I \in \mathbb{R}^{3\times3}$, $\mathbf{b}_I \in \mathbb{R}^3$, and $\mathbf{M} = [\,\mathbf{e}_1 \;\; \mathbf{e}_2\,]$. According to the geometry of the problem, it is possible to conclude that $\mathbf{Q}_I$ is invertible (it would be singular if and only if the camera mounted on the UAV were coincident with the sea surface, which is not possible). Thus ${}^Ix_b$and ${}^Iy_b$ verify

$$\begin{bmatrix}{}^Ix_b\\ {}^Iy_b\end{bmatrix} = \mathbf{M}^{\mathrm{T}}\mathbf{Q}_I^{-1}\mathbf{b}_I.$$

Through replacing the values of $\mathbf{m}$, ${}^I\mathbf{R}_p$, and ${}^I\mathbf{X}_p$ with the values of their measurements, the previous expression allows us to transform the measurements of (u, v), which depend nonlinearly on the state of the target, into the measurements $({}^Ix_{b_m}, {}^Iy_{b_m})$ of $({}^Ix_b, {}^Iy_b)$, which are a linear function of the state of the marine mammal.

In order to obtain estimates $[\,{}^I\hat{x}_b \;\; {}^I\hat{y}_b\,]^{\mathrm{T}}$ of the marine mammal's position $[\,{}^Ix_b \;\; {}^Iy_b\,]^{\mathrm{T}}$, consider a system with state $\mathbf{x}_I = \mathbf{x}_b = [\,{}^Ix_b \;\; {}^I\dot{x}_b \;\; {}^Iy_b \;\; {}^I\dot{y}_b\,]^{\mathrm{T}} \in \mathbb{R}^4$, whose evolution is governed by the linear stochastic difference equation (1), and consider that at a given instant of time t_k, measurements $\mathbf{z}_I(t_k) = [\,{}^Ix_{b_m}(t_k) \;\; {}^Iy_{b_m}(t_k)\,]^{\mathrm{T}} \in \mathbb{R}^2$ are available, given by

$$\mathbf{z}_I(t_k) = \underbrace{\begin{bmatrix}1 & 0 & 0 & 0\\ 0 & 0 & 1 & 0\end{bmatrix}}_{\mathbf{C}_I}\mathbf{x}_I(t_k) + \mathbf{v}_I(t_k). \tag{5}$$

The process noise $\mathbf{w}_I = \mathbf{w}_b$ and measurement noise $\mathbf{v}_I$ are assumed to be white, zero mean, Gaussian, and independent—$E[\mathbf{w}_I(t_k)\mathbf{v}_I^{\mathrm{T}}(t_j)] = 0$ for all t_k, t_j—and to have covariance matrices $\mathbf{Q}_I(\omega) = \mathbf{Q}_b(\omega)$ and $\mathbf{V}_I$, given, respectively, by (2) and $\mathbf{V}_I(t_k) = \mathrm{diag}[\,\sigma_{x_b}^2 \;\; \sigma_{y_b}^2\,]$, where σ_{x_b} and σ_{y_b} denote the standard deviations of the measurements ${}^Ix_{b_m}$ and${}^Iy_{b_m}$.

Let $\hat{\mathbf{x}}_I^-(t_k)$ and $\hat{\mathbf{x}}_I(t_k)$ denote a priori and a posteriori estimates of the state of the target, and $\mathbf{P}_I^-(t_k)$ and $\mathbf{P}_I(t_k)$ a priori and a posteriori state covariance matrices, respectively. The evolution of these quantities over time can be obtained according to a time-invariant KF defined by the following equations:

Predict step:

$$\begin{aligned}\hat{\mathbf{x}}_I^-(t_k) &= \mathbf{F}_I(\omega)\,\hat{\mathbf{x}}_I(t_{k-1})\\ \mathbf{P}_I^-(t_k) &= \mathbf{F}_I(\omega)\,\mathbf{P}_I(t_{k-1})\,\mathbf{F}_I^{\mathrm{T}}(\omega) + \mathbf{Q}_I(\omega).\end{aligned}$$

Update step:

$$\begin{aligned}\mathbf{K}_I(t_k) &= \mathbf{P}_I^-(t_k)\,\mathbf{C}_I^{\mathrm{T}}\left[\mathbf{C}_I\mathbf{P}_I^-(t_k)\,\mathbf{C}_I^{\mathrm{T}} + \mathbf{V}_I\right]^{-1}\\ \hat{\mathbf{x}}_I(t_k) &= \hat{\mathbf{x}}_I^-(t_k) + \mathbf{K}_I(t_k)\left(\mathbf{z}_I(t_k) - \mathbf{C}_I\hat{\mathbf{x}}_I^-(t_k)\right)\\ \mathbf{P}_I(t_k) &= [\mathbf{I}_4 - \mathbf{K}_I(t_k)\,\mathbf{C}_I]\,\mathbf{P}_I^-(t_k)\end{aligned} \tag{6}$$

(See [30, 31] for more details about Kalman filtering.) In these expressions, $\mathbf{F}_I(\omega)$ is the matrix that defines the dynamics of $\mathbf{x}_I$—i.e., $\mathbf{F}_I(\omega) = \mathbf{F}_b(\omega)$—and $t_k = kT$, with $k \in \mathbb{N}$. The state $\hat{\mathbf{x}}_{\mathbf{I}}(t_{k-1})$ and covariance $\mathbf{P}_I(t_{k-1})$ correspond to the initial conditions of the filter.

B. Joint KF

The isolated KF proposed in the previous section uses the measurements provided by the GPS receiver in the transformation of the measurements of (u, v) into measurements of $({}^Ix_b, {}^Iy_b)$, which depend linearly on the state of the target. In this section, a different approach is pursued: The measurements provided by the GPS are treated as regular sensor observations in the filtering process. A filter with a different structure results, and new estimates of the target state, as well as estimates of the UAV state, are provided.

From (4), it is straightforward to conclude that the value of λ can be obtained from

$$\lambda = \mathbf{e}_3^{\mathrm{T}}{}^p\mathbf{R}_c^{\mathrm{T}}\left[{}^I\mathbf{R}_p^{\mathrm{T}}\left({}^I\mathbf{X}_b - {}^I\mathbf{X}_p\right) - {}^p\mathbf{X}_c\right].$$

If this expression is substituted into (4), and the terms in the equation that results are reorganized, we have

$$\begin{aligned}&\left(\mathbf{A}_c^{-1}\mathbf{m}\mathbf{e}_3^{\mathrm{T}} - \mathbf{I}_3\right){}^p\mathbf{R}_c^{\mathrm{T}}{}^p\mathbf{X}_c\\ &\quad = \left(\mathbf{A}_c^{-1}\mathbf{m}\mathbf{e}_3^{\mathrm{T}} - \mathbf{I}_3\right){}^p\mathbf{R}_c^{\mathrm{T}}{}^I\mathbf{R}_p^{\mathrm{T}}\left({}^I\mathbf{X}_b - {}^I\mathbf{X}_p\right).\end{aligned}$$

Moreover, let $\mathbf{I}_n$ denote the identity matrix with dimension $n \times n$. If $\mathbf{M}$ is as defined as in the previous section, and $\mathbf{C}_b$ and $\mathbf{C}_p$ are given by $\mathbf{C}_b = [\,\mathbf{e}_1 \;\; \mathbf{0}_{3\times1} \;\; \mathbf{e}_2 \;\; \mathbf{0}_{3\times1}\,]$ and $\mathbf{C}_p = \mathbf{I}_3 \otimes \mathbf{e}_1^{\mathrm{T}}$ (where $\mathbf{0}_{n\,\times\,m}$ is a matrix of 0s with dimension $n \times m$), the previous system, which has three equations, can be cast into the form

$$\begin{aligned}&\underbrace{\mathbf{M}^{\mathrm{T}}\left(\mathbf{A}_c^{-1}\mathbf{m}\mathbf{e}_3^{\mathrm{T}} - \mathbf{I}_3\right){}^p\mathbf{R}_c^{\mathrm{T}}{}^p\mathbf{X}_c}_{\mathbf{y}}\\ &\quad = \mathbf{M}^{\mathrm{T}}\left(\mathbf{A}_c^{-1}\mathbf{m}\mathbf{e}_3^{\mathrm{T}} - \mathbf{I}_3\right){}^p\mathbf{R}_c^{\mathrm{T}}{}^I\mathbf{R}_p^{\mathrm{T}}\left(\mathbf{C}_b\mathbf{x}_b - \mathbf{C}_p\mathbf{x}_p\right),\end{aligned}$$

which is a system with two equations. The third equation was removed since the last row of $\mathbf{A}_c^{-1}\mathbf{m}\mathbf{e}_3^{\mathrm{T}} - \mathbf{I}_3$ is a vector of 0s. If the value of $\mathbf{m}$ in the previous expression is replaced by the value of its measurements, the measurements of (u, v), which are a nonlinear function of the state of the target, are transformed into measurements $\mathbf{y}_m, \mathbf{y} \in \mathbb{R}^2$, which depend linearly on the state $\mathbf{x}_b$ of the target and on the state $\mathbf{x}_p$ of the UAV.

If the state of the new system is considered to be $\mathbf{x}_J = [\,\mathbf{x}_b^{\mathrm{T}}\ \mathbf{x}_p^{\mathrm{T}}\,]^{\mathrm{T}} \in \mathbb{R}^{13}$, then at time t_k the relation between the measurements $\mathbf{z}_J(t_k) = [\,\mathbf{y}_m^{\mathrm{T}}(t_k)\quad {}^I\mathbf{X}_{p_m}^{\mathrm{T}}(t_k)\,]^{\mathrm{T}} \in \mathbb{R}^5$ and the state of the system is given by

$$\mathbf{z}_J(t_k) = \mathbf{C}_J(t_k)\,\mathbf{x}_J(t_k) + \mathbf{v}_J(t_k), \tag{7}$$

where $\mathbf{C}_J(t_k)$ has the form

$$\mathbf{C}_J(t_k) = \begin{bmatrix} \mathbf{M}^{\mathrm{T}}\big(\mathbf{A}_c^{-1}\mathbf{m}(t_k)\,\mathbf{e}_3^{\mathrm{T}} - \mathbf{I}_3\big)^p\mathbf{R}_c^{\mathrm{T}\,I}\mathbf{R}_p^{\mathrm{T}}(t_k) & \mathbf{0}_{2\times 3} \\ \mathbf{0}_{3\times 3} & \mathbf{I}_3 \end{bmatrix} \times \begin{bmatrix} \mathbf{C}_b & -\mathbf{C}_p \\ \mathbf{0}_{3\times 4} & \mathbf{C}_p \end{bmatrix}.$$

The values of $\mathbf{y}_m(t_k)$, ${}^I\mathbf{X}_{p_m}(t_k)$, and $\mathbf{v}_J(t_k)$ denote the measurements of $\mathbf{y}$, ${}^I\mathbf{X}_p$, and the measurement noise, respectively, at instant t_k. Since both $\mathbf{m}$ and ${}^I\mathbf{R}_p$ depend on time, in this case the measurements equation is time varying.

The state $\mathbf{x}_J$ of the system results from the concatenation of the state of the target and the state of the UAV; therefore its evolution over time is modeled by the linear stochastic difference equation

$$\mathbf{x}_J(t_k) = \underbrace{\begin{bmatrix} \mathbf{F}_b(\omega) & \mathbf{0}_{4\times 9} \\ \mathbf{0}_{9\times 4} & \mathbf{F}_p \end{bmatrix}}_{\mathbf{F}_J(\omega)} \mathbf{x}_J(t_{k-1}) + \underbrace{\begin{bmatrix} \mathbf{w}_b(t_{k-1}) \\ \mathbf{w}_p(t_{k-1}) \end{bmatrix}}_{\mathbf{w}_J(t_{k-1})}.$$

The process noise $\mathbf{w}_J$ and measurement noise $\mathbf{v}_J$ are assumed to be white, zero mean, Gaussian, and independent—$E[\mathbf{w}_J(t_k)\mathbf{v}_J^{\mathrm{T}}(t_j)] = 0$ for all t_k, t_j—and to have covariance matrices $\mathbf{Q}_J(\omega)$ and $\mathbf{V}_J$, respectively, of the forms

$$\mathbf{Q}_J(\omega) = \begin{bmatrix} \mathbf{Q}_b(\omega) & \mathbf{0}_{4\times 9} \\ \mathbf{0}_{9\times 4} & \mathbf{Q}_p \end{bmatrix}$$

and

$$\mathbf{V}_J = \begin{bmatrix} \mathbf{V}_{\mathbf{y}_m} & \mathbf{0}_{2\times 3} \\ \mathbf{0}_{3\times 2} & \mathbf{V}_p \end{bmatrix},$$

where $\mathbf{V}_{\mathbf{y}_m} \in \mathbb{R}^{2\times 2}$ and $\mathbf{V}_p \in \mathbb{R}^{3\times 3}$ are diagonal matrices with the variances of the components of $\mathbf{y}_m$ and ${}^I\mathbf{X}_{p_m}$ in their respective diagonals.

Using a reasoning and notation similar to the ones at the end of Section III-A, a joint KF is obtained that estimates the state of the target and the state of the UAV. Since the measurements equation in (7) is time varying, in contrast to the time-invariant equation in (5), when replacing the value of $\mathbf{C}_I$ in (6) with the value of $\mathbf{C}_J$, attention must be paid to the fact that $\mathbf{C}_J$ is time varying—i.e., $\mathbf{C}_I$ must be replaced by $\mathbf{C}_J(t_k)$. All other substitutions are straightforward.

According to the strategy already described, the estimates $[\,{}^I\hat{x}_b(t_k)\quad {}^I\hat{y}_b(t_k)\,]^{\mathrm{T}}$ for the position $[\,{}^Ix_b\quad {}^Iy_b\,]^{\mathrm{T}}$ of the target at a given instant t_k can be obtained from the first and third entries of $\hat{\mathbf{x}}_{\mathbf{J}}(t_k)$. Moreover, estimates for the position of the UAV with respect to the inertial reference frame at the same instant can be obtained from the fifth, eighth, and 11th entries of $\hat{\mathbf{x}}_{\mathbf{J}}(t_k)$.

C. Multiple-Model Adaptive Estimation

The model considered for the marine mammal—see (1)—assumes that its angular speed is known, which is not a realistic assumption. In order to overcome this issue, an approach is used based on the use of multiple models, which simultaneously identifies some parameters of the system and estimates its state. In particular, the strategy implemented in this work, known as MMAE [7], consists in considering several models for a system that differ in a set of parameters (in this case the target angular speed). For each of these models, an isolated (see Section III-A) or joint (see Section III-B) KF is designed, depending on the strategy in use. The estimates provided by each individual filter are then combined, using a posteriori probabilities as weighting factors, to obtain final estimates for the state of the system and for the associated error covariance matrix. These probabilities are computed from the residuals of each filter, and measure the proximity between each model and the true one. The MMAE based on the bank of isolated KFs is here referred to as isolated MMAE, and the one based on the bank of joint KFs is referred to as joint MMAE. Both methods provide estimates for the position of a marine mammal moving at the sea surface with an unknown angular speed.

If N models are considered, the a posteriori hypothesis probability of the ith model, $i = 1, \ldots, N$, evolves over time from an initial estimate p_0^i according to

$$p_k^i = \frac{\beta_k^i e^{-\frac{1}{2}\psi_k^i}}{\sum_{j=1}^{N} \beta_k^j e^{-\frac{1}{2}\psi_k^j}\, p_{k-1}^j}\, p_{k-1}^i,$$

where

$$\beta_k^i = \frac{1}{(2\pi)^{m/2}\sqrt{\det\left(\mathbf{S}_k^i\right)}}.$$

$$\psi_k^i = \left(\mathbf{r}_k^i\right)^{\mathrm{T}}\left(\mathbf{S}_k^i\right)^{-1}\mathbf{r}_k^i$$

$$\mathbf{r}_k^i = \mathbf{z}_k - (\mathbf{z}_{\bar{k}})^i$$

$$\mathbf{S}_k^i = \mathbf{C}_k^i(\mathbf{P}_{\bar{k}})^i\left(\mathbf{C}_k^i\right)^{\mathrm{T}} + \mathbf{V}^i$$

(See [7] for details.) Moreover, $\mathbf{r}^i$ is the residual vector of the ith KF—the difference between the sensor measurements $\mathbf{z}$ and the measurements $(\mathbf{z}^-)^i$ predicted by model i; $\mathbf{S}^i$ is the residual covariance matrix associated with the ith KF; and m is the number of measurements. For the sake of clarity, in this section the time instant t_k is represented by the subscript k. The values of $\mathbf{C}^i$, $\mathbf{V}^i$, and

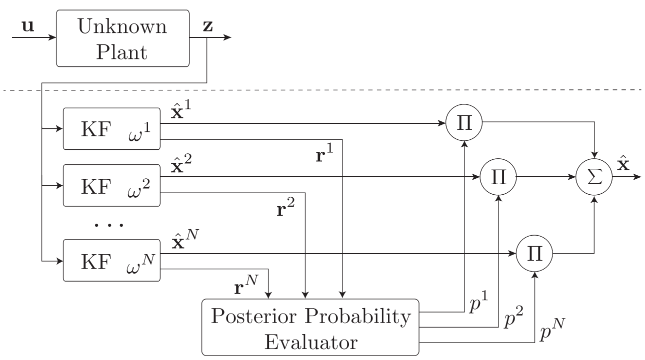

Fig. 2. Structure of multiple-model adaptive estimators.

$(\mathbf{P}^-)^i$ correspond, respectively, to the values of the matrices $\mathbf{C}$, $\mathbf{V}$, and $\mathbf{P}^-$ of the ith KF of the MMAE under consideration, i.e., either the isolated or the joint MMAE.

From the individual state estimates provided by each KF, their error covariance matrices, and the a posteriori probability of each hypothesis, it is possible to compute the weighted state estimate

$$\hat{\mathbf{x}}_k = \sum_{j=1}^{N} p_k^j \hat{\mathbf{x}}_k^j$$

and the global covariance matrix

$$\mathbf{P}_k = \sum_{j=1}^{N} p_k^j \left[\mathbf{P}_k^j + \left(\hat{\mathbf{x}}_k^j - \hat{\mathbf{x}}_k\right)\left(\hat{\mathbf{x}}_k^j - \hat{\mathbf{x}}_k\right)^{\mathrm{T}}\right].$$

In these expressions, $\hat{\mathbf{x}}^j$ and $\mathbf{P}^j$ denote, respectively, the a posteriori state estimate and a posteriori state covariance matrix of the jth KF. Let ω^j, $j = 1, 2, \ldots, N$, denote the angular speed of such a filter, and $\mathbf{u}$ the unknown input that drives the motion of the target. In this case, the structure of the proposed estimators is the one in Fig. 2.

The use of multiple-model approaches requires the definition of a criterion to divide the parameter set into smaller parameter subsets. (In [6], for instance, where this problem was addressed from the control point of view, this division and the specification of the number of models that should be used were based on the definition of performance requirements for the controller.) Once the number of models is determined, the subsets associated with each model must be computed, as well as the nominal angular-speed values for each individual filter. With this purpose, the BPM is usually adopted, but techniques based on the Kullback information metric can also be found in the literature (see [28, 31], respectively, for details).

If a KF is designed using the actual angular-speed value, its steady-state residual $\mathbf{r}^*$ is stationary white noise, with a given covariance matrix, here denoted $\mathbf{S}^*$. Let ω denote the actual value of the unknown parameter and ω^i the nominal parameter value used to implement the ith KF. If $\omega^i = \omega$, the steady-state residual $\mathbf{r}^i$ of the ith KF is also stationary white noise with covariance matrix $\mathbf{S}^*$. On the other hand, if $\omega^i \neq \omega$ this residual is not white. The BPM is a function that measures the stochastic distance between the residuals $\mathbf{r}^*$ and $\mathbf{r}^i$, and can be computed using the expression

$$L_*^i \equiv \log\left[\det\left(\mathbf{S}^i\right)\right] + \mathrm{tr}\left[\left(\mathbf{S}^i\right)^{-1}\boldsymbol{\Gamma}_*^i\right], \tag{8}$$

where L_*^i denotes the BPM between the ith filter and the filter based upon the true model, $\boldsymbol{\Gamma}_*^i$ denotes the actual steady-state prediction error covariance of the residual of the ith filter computed using information about the true model, and $\mathbf{S}^i$ denotes the steady-state covariance of the residual of the ith filter. A detailed derivation of (8) and a description of the use of the BPM in multiple-model architectures can be found in [6, 28].

In order to find the number of models to use and the corresponding nominal parameter values, let the null angular speed, which corresponds to straight or parabolic trajectories, be the nominal parameter of one of the models. Then search the remaining parameter set for the angular-speed nominal values that lead to a situation in which there is always a filter whose BPM with respect to the filter based upon the true model does not exceed a certain value. The boundaries of each subset are defined by the points of intersection of the BPM curves. In this case, a total of $N = 4$ models results, with the nominal angular-speed values presented at the end of this section.

According to the fundamental convergence result, proved in [28] for an arbitrary number of stable KFs, if the BPM from the true model to one of the nominal models is smaller than its BPM to any other model, then under some additional stationarity conditions and ergodicity assumptions the a posteriori probabilities will converge almost surely to the correct model (see [6, 28] and references therein for formal proofs and precise definitions of these concepts).

In this case, as in most target-tracking applications, the model of the target is unstable, and thus the strategy previously described does not provide theoretical guarantees of convergence for the correct model. Such a strategy is used here only to gain some insight into how to choose the angular-speed nominal values for each KF. With this purpose, a set of simulations were carried out in which the value of the BPM was obtained from $\boldsymbol{\Gamma}_*^i$, which was computed as being a correlation matrix rather than a covariance matrix, since the mean of the residuals of the filters is not negligible (recall that the model of the target is unstable).

Fig. 3 depicts the BPM for each of the four models obtained for the isolated MMAE. For the joint strategy, the same models are considered. The four angular-speed nominal values used to design the KFs are the ones that minimize the BPMs presented in Fig. 3—[0 0.02 0.040.06] rad/s—which lead to the division of the original set ($\Omega = [0, 0.07]$ rad/s) into the following subsets:

$$\Omega_1 = [0, 0.01]\,\mathrm{rad/s}$$
$$\Omega_2 = [0.01, 0.03]\,\mathrm{rad/s}$$
$$\Omega_3 = [0.03, 0.05]\,\mathrm{rad/s}$$
$$\Omega_4 = [0.05, 0.07]\,\mathrm{rad/s}.$$

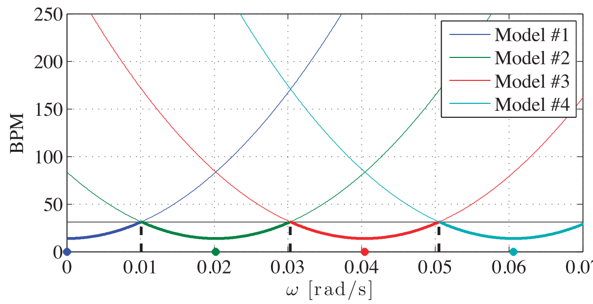

Fig. 3. BPM for four models. Dots in different colors correspond to angular-speed values that minimize BPM in each subset.

As can be seen, the regions of validity of the four subsets have similar dimensions, and thus in this particular situation the use of the BPM and of a strategy based on the Euclidean distance between the four nominal angular-speed values would lead to approximately the same results.

D. Extended KF

In order to compare the two filters proposed in the previous sections with a standard approach, an EKF is presented in this section that estimates the state of the target, its angular speed, and the state of the UAV. For each problem, several different EKF-based architectures can be designed, leading to different performances and computational demands. Since the EKF presented in this work is provided only for comparison purposes, its classical version is implemented (see [30]). Interested readers are referred to [32, 33] for different architectures and developments regarding this type of filter.

If the state of the system is the concatenation of the state of the target with its angular speed and with the state of the UAV, $\mathbf{x}_e = [\,\mathbf{x}_b^{\mathrm{T}}\ \omega\ \mathbf{x}_p^{\mathrm{T}}\,]^{\mathrm{T}} \in \mathbb{R}^{14}$, then its temporal evolution is given by the nonlinear stochastic difference equation

$$\begin{aligned}\mathbf{x}_e(t_k) &= f_e(\mathbf{x}_e(t_{k-1})) + \mathbf{w}_e(t_{k-1})\\ &= \begin{bmatrix}\mathbf{F}_b(\omega(t_{k-1})) & \mathbf{0}_{4\times1} & \mathbf{0}_{4\times9}\\ \mathbf{0}_{1\times4} & 1 & \mathbf{0}_{1\times9}\\ \mathbf{0}_{9\times4} & \mathbf{0}_{9\times1} & \mathbf{F}_p\end{bmatrix}\\ &\quad\times \mathbf{x}_e(t_{k-1}) + \mathbf{w}_e(t_{k-1}),\end{aligned}$$

where $\mathbf{w}_e(t_{k-1}) = [\,\mathbf{w}_b^{\mathrm{T}}(t_{k-1})\ \mathrm{w}_\omega(t_{k-1})\ \mathbf{w}_p^{\mathrm{T}}(t_{k-1})\,]^{\mathrm{T}} \in \mathbb{R}^{14}$ and f_e is a nonlinear function of the state. The angular speed is modeled as a Wiener sequence [23], as its increments $\mathrm{w}_\omega(t_{k-1})$ are assumed to be an independent (white-noise) process.

Moreover, let the measurements $\mathbf{z}_e(t_k) \in \mathbb{R}^5$ available at instant t_k be given by

$$\begin{aligned}\mathbf{z}_e(t_k) &= h_e(\mathbf{x}_e(t_k)) + \mathbf{v}_e(t_k),\\ &= \begin{bmatrix}\mathbf{M}^{\mathrm{T}}\mathbf{m}(t_k)\\ {}^{I}\mathbf{X}_p(t_k)\end{bmatrix} + \mathbf{v}_e(t_k)\end{aligned}$$

where h_e is a nonlinear function of the state of the system and $\mathbf{v}_e(t_k) \in \mathbb{R}^5$ is the measurement noise. If $\mathbf{C}_e = [\,\mathbf{C}_b\ \mathbf{0}_{3\times1}\ -\mathbf{C}_p\,]$, then according to (4) it is possible to conclude that

$$h_e(\mathbf{x}_e(t_k)) = \begin{bmatrix}\dfrac{\mathbf{M}^{\mathrm{T}}\mathbf{A}_c{}^{p}\mathbf{R}_c^{\mathrm{T}}\left({}^{I}\mathbf{R}_p^{\mathrm{T}}(t_k)\,\mathbf{C}_e\mathbf{x}_e(t_k) - {}^{p}\mathbf{X}_c\right)}{\mathbf{e}_3^{\mathrm{T}}{}^{p}\mathbf{R}_c^{\mathrm{T}}\left({}^{I}\mathbf{R}_p^{\mathrm{T}}(t_k)\,\mathbf{C}_e\mathbf{x}_e(t_k) - {}^{p}\mathbf{X}_c\right)}\\ {}^{I}\mathbf{X}_p(t_k)\end{bmatrix}.$$

The Jacobian matrix $\mathbf{F}_e$ of f_e has the form

$$\mathbf{F}_e(\hat{\mathbf{x}}_e(t_k)) = \begin{bmatrix}\mathbf{F}_b(\hat{\omega}(t_k)) & \mathbf{a}_e(\hat{\mathbf{x}}_e(t_k)) & \mathbf{0}_{4\times9}\\ \mathbf{0}_{1\times4} & 1 & \mathbf{0}_{1\times9}\\ \mathbf{0}_{9\times4} & \mathbf{0}_{9\times1} & \mathbf{F}_p\end{bmatrix},$$

where $\mathbf{a}_e(\hat{\mathbf{x}}_e(t_k)) \in \mathbb{R}^4$ is given by

$$\mathbf{a}_e(\hat{\mathbf{x}}_e(t_k)) = \begin{bmatrix}\dfrac{\hat{\mathbf{x}}_{e_2}(t_k)\,[T\hat{\omega}(t_k)\cos(T\hat{\omega}(t_k)) - \sin(T\hat{\omega}(t_k))] - \hat{\mathbf{x}}_{e_4}(t_k)\,[T\hat{\omega}(t_k)\sin(T\hat{\omega}(t_k)) - 1 + \cos(T\hat{\omega}(t_k))]}{\hat{\omega}^2(t_k)}\\ -\hat{\mathbf{x}}_{e_2}(t_k)\,T\sin(T\hat{\omega}(t_k)) - \hat{\mathbf{x}}_{e_4}(t_k)\,T\cos(T\hat{\omega}(t_k))\\ \dfrac{\hat{\mathbf{x}}_{e_2}(t_k)\,[T\hat{\omega}(t_k)\sin(T\hat{\omega}(t_k)) - 1 + \cos(T\hat{\omega}(t_k))] + \hat{\mathbf{x}}_{e_4}(t_k)\,[T\hat{\omega}(t_k)\cos(T\hat{\omega}(t_k)) - \sin(T\hat{\omega}(t_k))]}{\hat{\omega}^2(t_k)}\\ \hat{\mathbf{x}}_{e_2}(t_k)\,T\cos(T\hat{\omega}(t_k)) - \hat{\mathbf{x}}_{e_4}(t_k)\,T\sin(T\hat{\omega}(t_k))\end{bmatrix}.$$

Moreover, the vector $\hat{\mathbf{x}}_e(t_k) = [\,\hat{\mathbf{x}}_b^{\mathrm{T}}(t_k)\ \hat{\omega}(t_k)\ \hat{\mathbf{x}}_p^{\mathrm{T}}(t_k)\,]^{\mathrm{T}}$ is the estimate for the state $\mathbf{x}_e(t_k)$ of the system at instant t_k; and $\hat{\mathbf{x}}_b^{\mathrm{T}}(t_k)$, $\hat{\omega}(t_k)$, and $\hat{\mathbf{x}}_p^{\mathrm{T}}(t_k)$ are estimates for the state of the target, its angular speed, and the UAV, respectively, at the same time instant. In the expressions, $\hat{\mathbf{x}}_{e_i}(t_k)$, $i = 1, 2, \ldots, 14$, denotes the ith entry of $\hat{\mathbf{x}}_e(t_k)$. The Jacobian $\mathbf{H}_e$ of h_e is given by

$$\mathbf{H}_e(\hat{\mathbf{x}}_e(t_k)) = \begin{bmatrix}\mathbf{M}^{\mathrm{T}}\mathbf{A}_c{}^{p}\mathbf{R}_c^{\mathrm{T}}\dfrac{{}^{I}\mathbf{R}_p^{\mathrm{T}}(t_k)\,\mathbf{C}_e\left[\mathbf{e}_3^{\mathrm{T}}{}^{p}\mathbf{R}_c^{\mathrm{T}}\left({}^{I}\mathbf{R}_p^{\mathrm{T}}(t_k)\,\mathbf{C}_e\hat{\mathbf{x}}_e(t_k) - {}^{p}\mathbf{X}_c\right)\right] - \left({}^{I}\mathbf{R}_p^{\mathrm{T}}(t_k)\,\mathbf{C}_e\hat{\mathbf{x}}_e(t_k) - {}^{p}\mathbf{X}_c\right)\left[\mathbf{e}_3^{\mathrm{T}}{}^{p}\mathbf{R}_c^{\mathrm{T}}{}^{I}\mathbf{R}_p^{\mathrm{T}}(t_k)\,\mathbf{C}_e\right]}{\left[\mathbf{e}_3^{\mathrm{T}}{}^{p}\mathbf{R}_c^{\mathrm{T}}\left({}^{I}\mathbf{R}_p^{\mathrm{T}}(t_k)\,\mathbf{C}_e\hat{\mathbf{x}}_e(t_k) - {}^{p}\mathbf{X}_c\right)\right]^2}\\ \mathbf{0}_{3\times5}\quad \mathbf{C}_p\end{bmatrix}.$$

Let the a priori and a posteriori state estimates be denoted by $\hat{\mathbf{x}}_e^-(t_k)$ and $\hat{\mathbf{x}}_e(t_k)$, and the a priori and a posteriori state covariance matrices by $\mathbf{P}_e^-(t_k)$ and $\mathbf{P}_e(t_k)$, respectively. According to this notation, an EKF that estimates the state $\mathbf{x}_e(t_k)$ of the system is given by the following set of equations:

Predict step:

$$\begin{aligned}\hat{\mathbf{x}}_e^-(t_k) &= f_e\left(\hat{\mathbf{x}}_e(t_{k-1})\right)\\ \mathbf{P}_e^-(t_k) &= \mathbf{F}_e\left(\hat{\mathbf{x}}_e(t_{k-1})\right)\mathbf{P}_e(t_{k-1})\mathbf{F}_e^{\mathrm{T}}\left(\hat{\mathbf{x}}_e(t_{k-1})\right) + \mathbf{Q}_e\left(\omega^*\right)\end{aligned}$$

Update step:

$$\begin{aligned}\mathbf{S}_e(t_k) &= \mathbf{H}_e\left(\hat{\mathbf{x}}_e^-(t_k)\right)\mathbf{P}_e^-(t_k)\mathbf{H}_e^{\mathrm{T}}\left(\hat{\mathbf{x}}_e^-(t_k)\right) + \mathbf{V}_e\\ \mathbf{K}_e(t_k) &= \mathbf{P}_e^-(t_k)\mathbf{H}_e^{\mathrm{T}}\left(\hat{\mathbf{x}}_e^-(t_k)\right)\mathbf{S}_e^{-1}(t_k)\\ \hat{\mathbf{x}}(t_k) &= \hat{\mathbf{x}}_e^-(t_k) + \mathbf{K}_e(t_k)\left[\mathbf{z}_e(t_k) - h_e\left(\hat{\mathbf{x}}_e^-(t_k)\right)\right]\\ \mathbf{P}_e(t_k) &= \left[\mathbf{I}_{14} - \mathbf{K}_e(t_k)\mathbf{H}_e\left(\hat{\mathbf{x}}_e^-(t_k)\right)\right]\mathbf{P}_e^-(t_k)\end{aligned}$$

where $\mathbf{S}_e(t_k)$ is the residual covariance matrix and the matrices $\mathbf{Q}_e(\omega^*)$ and $\mathbf{V}_e$ are, respectively, the covariances of the process noise $\mathbf{w}_e$ and measurement noise $\mathbf{v}_e$, which are assumed to be white, Gaussian, and zero mean. These matrices have the forms

$$\mathbf{Q}_e\left(\omega^*\right) = \begin{bmatrix}\mathbf{Q}_b(\omega^*) & \mathbf{0}_{4\times1} & \mathbf{0}_{4\times9}\\ \mathbf{0}_{1\times4} & Q_\omega & \mathbf{0}_{1\times9}\\ \mathbf{0}_{9\times4} & \mathbf{0}_{9\times1} & \mathbf{Q}_p\end{bmatrix},$$

$$\mathbf{V}_e = \begin{bmatrix}\mathbf{V}_{\mathbf{y}_e} & \mathbf{0}_{2\times3}\\ \mathbf{0}_{3\times2} & \mathbf{V}_p\end{bmatrix}$$

where $\mathbf{V}_{\mathbf{y}_e} \in \mathbb{R}^{2\times2}$ is a diagonal matrix with the variances of the first two entries of $\mathbf{z}_e$ in its diagonal and $\mathbf{V}_p \in \mathbb{R}^{3\times3}$ is a diagonal matrix with the variances of the three components of ${}^I\mathbf{X}_{p_m}$ in its diagonal. In these expressions, $\mathbf{Q}_b$ and $\mathbf{Q}_p$ are defined as in Section II, $Q_\omega \in \mathbb{R}$ is the variance of the noise w_ω that affects the target angular speed, and ω^* is an arbitrary angular-speed value which is assumed to be in the center of the interval to which the target angular speed is considered to belong. The state $\hat{\mathbf{x}}_{\mathbf{e}}(t_{k-1})$ and covariance $\mathbf{P}_e(t_{k-1})$ correspond to the initial conditions of the filter. See [30] for more details about EKFs.

IV. SIMULATION RESULTS

In this section, simulation results are presented that illustrate and compare the performance of the filters proposed in the previous sections. Experiments depicting their behavior when the marine mammal submerges are also provided.

In order to keep the simulations as realistic as possible, the trajectories described by the UAV are generated according to the aircraft dynamic model SymAirDyn, proposed in [4]. The image-acquisition module is modeled by a pinhole camera with position ${}^P\mathbf{X}_c = (\,200\ 0\ 100\,)$ mm and orientation ${}^P\mathbf{R}_c = {}^P\mathbf{R}_{c_0}\mathbf{R}(\alpha_p)\mathbf{R}(\theta_p)$ with respect to $\{P\}$, where $\mathbf{R}(\alpha_p)$, $\mathbf{R}(\theta_p)$, and ${}^P\mathbf{R}_{c_0}$ are rotation matrices that express rotations of α_p, θ_p, and $-\pi/2$ rad about the x-, y-, and z-axes, respectively. In these expressions, $\mathbf{R}(\alpha_p)$ and $\mathbf{R}(\theta_p)$ denote the rotation matrices that express the camera pan and tilt movements (α_p and θ_p denote the camera pan and tilt angles, respectively), and ${}^P\mathbf{R}_{c_0}$ corresponds to the orientation of the camera with respect to $\{P\}$ when $\alpha_p = \theta_p = 0$ rad. The camera control strategy proposed by the authors in [34] can be used to keep the target visible in the images.

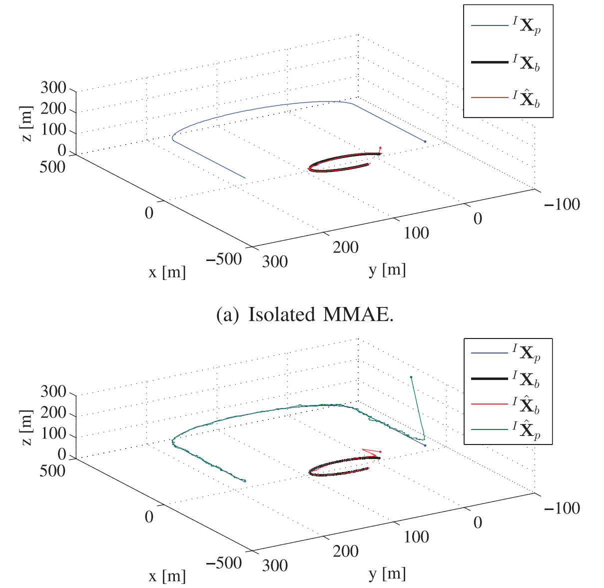

(a) Isolated MMAE.

(b) Joint MMAE.

Fig. 4. Evolution over time of actual and estimated positions of marine mammal and UAV when mammal moves with angular speed of third model.

In the simulations reported in this section, the sampling interval is $T = 0.2$ s and the marine mammal's angular speed is considered to belong to the interval [0, 0.07] rad/s. The covariance matrices $\mathbf{Q}_b$ and $\mathbf{Q}_p$, obtained from the power spectral densities $S_{w_b} = 10^{-3}$ m^2/s^3 and $S_{w_p} = 10^{-1}$ m^2/s^5, are used, as well as $Q_\omega = 10^{-8}$ rad^2/s^2. Regarding the covariance of the measurements, we have $\mathbf{V}_I = \mathbf{V}_{\mathbf{y}_m} = 10^2\mathbf{I}_2$ m^2, $\mathbf{V}_{\mathbf{y}_e} = 5^2\mathbf{I}_2$ pixels squared, and $\mathbf{V}_p = 10^2\mathbf{I}_3$ m^2. The measurements of the yaw, pitch, and roll angles of the UAV, provided by the AHRS, are corrupted by zero-mean, white, and Gaussian noises, with standard deviation 0.5°, 0.2°, and 0.2°, respectively. A significant error is included in the initial conditions of the state of the three filters. In the case of the two MMAEs, the initial probabilities associated with each of the four models are assumed to be equal, i.e., 1/4.

In Fig. 4, the actual positions of the marine mammal ${}^I\mathbf{X}_b$ and UAV ${}^I\mathbf{X}_p$ are depicted for an experiment where the marine mammal describes a circular trajectory with the angular speed associated with the third model, i.e., $\omega = 0.04$ rad/s. The UAV moves along the trajectory depicted in blue. The time evolution of the target position estimates ${}^I\hat{\mathbf{X}}_b$, provided by both the isolated and joint filters, is also depicted, as well as the evolution of the estimates of the UAV position ${}^I\hat{\mathbf{X}}_p$ provided by the joint filtering approach.

The performance of the isolated and joint filters is illustrated in Fig. 5. For comparison purposes, the results obtained with the EKF presented in Section III-D are also

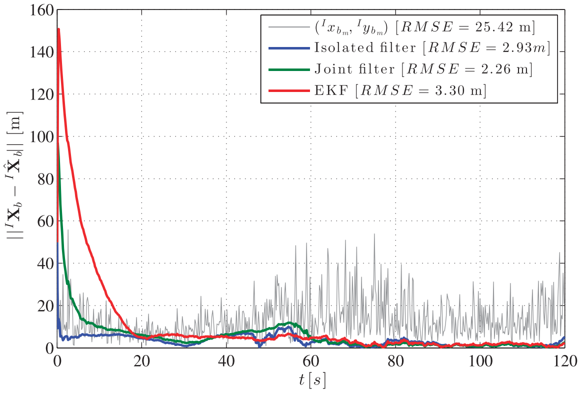

Fig. 5. Euclidean norm of marine mammal's position estimation error when mammal moves with angular speed of third model. Values in brackets are steady-state RMSEs of position estimates provided by each strategy.

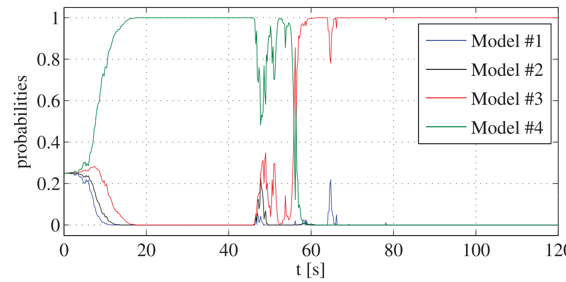

(a) Isolated MMAE.

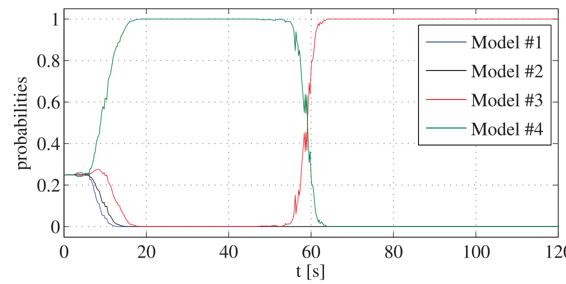

(b) Joint MMAE.

Fig. 6. Evolution over time of a posteriori probabilities of each model when actual model is third.

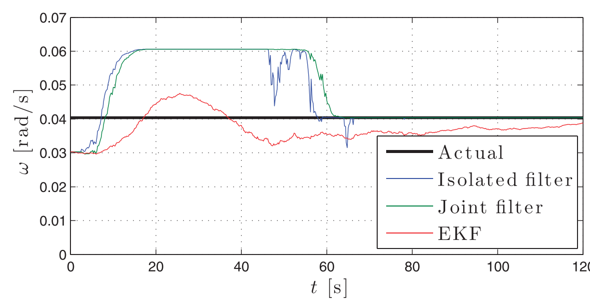

Fig. 7. Evolution over time of estimates for angular speed of marine mammal when actual angular-speed value is 0.04 rad/s.

depicted, as well as the measurements ${}^I x_{b_m}$ and ${}^I y_{b_m}$ of the marine mammal's position, which are computed using the strategy described in Section III-A. The estimates provided by the three filters converge to the vicinity of the actual target position. Even though in this experiment the steady-state performance of the filters is similar (their root mean square errors [RMSEs] are close to each other), the performance of the joint MMAE is better than those achieved by the other two filters. In the case of the isolated MMAE, this result is a consequence of its structure, since the transformation applied to the observations depends on the measurements of the position of the UAV, which are not exact. In the case of the EKF, performance is conditioned by the model of the target, which is highly nonlinear on its angular speed—see (1). From Fig. 5 it is also possible to conclude that the three presented filters lead to significant improvements in terms of performance in the estimation of the position of the marine mammal, when compared to the direct use of the measurements ${}^I x_{b_m}$ and ${}^I y_{b_m}$ of the marine mammal's position.

In this experiment, the main source of errors is the high altitude of the UAV with respect to the mammal's position. The UAV moves 150 m above the sea surface, and thus small uncertainties in the measurements of its attitude, and consequently in the measurements of the attitude of the camera, have a significant impact on the estimates of the position of the target.

Results regarding the identification of the actual model of the marine mammal are depicted in Figs. 6 and 7. As expected, the a posteriori probability of the third model, which is the one that considers the real angular-speed value, converges to 1 after the initial transient, when both the isolated and joint MMAEs are used. This leads to the correct identification of the angular speed of the target ($\omega = 0.04$ rad/s; Fig. 7). The angular-speed estimates are obtained by combining the angular speeds associated with each of the four models through a weighted sum, with the a posteriori hypothesis probabilities of each model used as weighting factors.

A special type of trajectory appears when the marine mammal moves along a straight line—i.e., when its angular speed is null. An experiment that reports this situation is presented in Figs. 8–10. If the trajectories of the marine mammal and UAV are the ones presented in Fig. 8, the performance of the isolated and joint filters, and the performance of the EKF, are the ones presented in Fig. 9. Note that the trajectory of the UAV is the same as before (see Figs. 4 and 8), as the proposed approaches do not impose any constraints on the motion of the UAV. As can be seen from Fig. 9, the position estimates provided by the three filters converge to the vicinity of the mammal's real position, and the joint filter is the one that leads to the best steady-state accuracy, followed by the isolated filter and EKF, respectively, similar to what occurred in the previous experiment.

The angular-speed estimates provided by the three filters are depicted in Fig. 10. As can be seen, the estimates provided by the isolated and joint filters converge to the real angular-speed value, $\omega = 0$ rad/s,

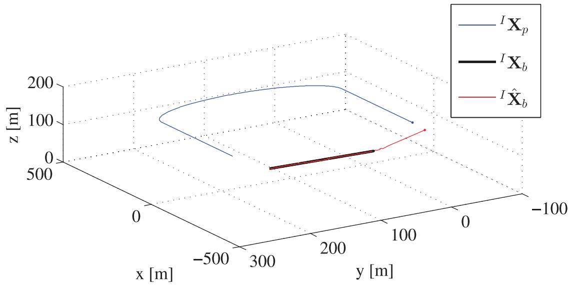

(a) Isolated MMAE.

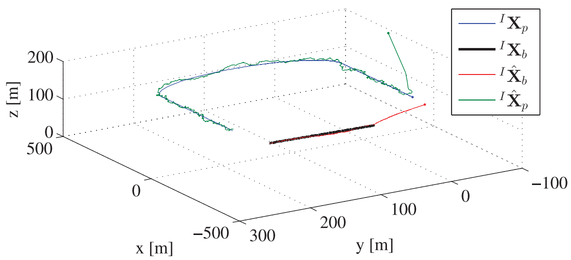

(b) Joint MMAE.

Fig. 8. Evolution over time of actual and estimated positions of marine mammal and UAV when mammal moves along straight line (i.e., with null angular speed).

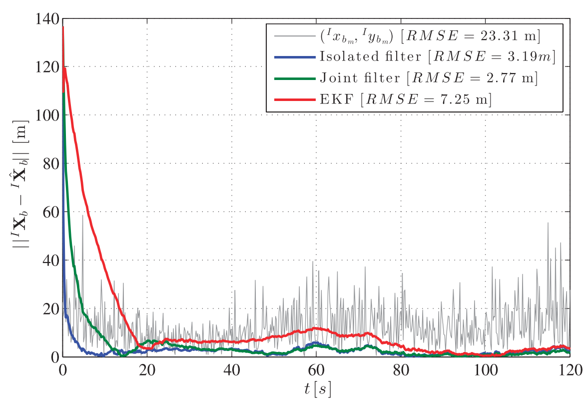

Fig. 9. Euclidean norm of marine mammal's position estimation error when mammal moves along straight line. Values in brackets are steady-state RMSEs of position estimates provided by each strategy.

although in this case the rate of convergence of the EKF is slower than those of the two proposed estimators. This degradation in the performance of the EKF was somewhat expected, as straight trajectories are typically more challenging for positioning and tracking systems. Such degradation is not observed in the performance of the joint and isolated filters, as both include a model for the particular case of null angular speeds.

Fig. 11 assesses the performance of the three filters in terms of the estimation of the position of a marine mammal that moves according to the trajectory in Fig. 4 and submerges during the time interval [60, 90] s. During this period, estimates of the position of the marine mammal are obtained by resorting only to the prediction step of the filters, as measurements of the center of the target are not available from the images. As can be seen, the performance of the isolated and joint MMAEs is

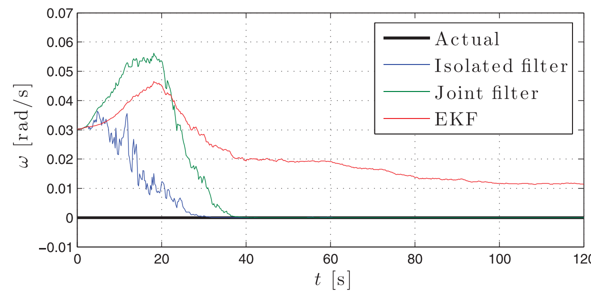

Fig. 10. Evolution over time of estimates for angular speed of marine mammal when actual angular-speed value is 0 rad/s.

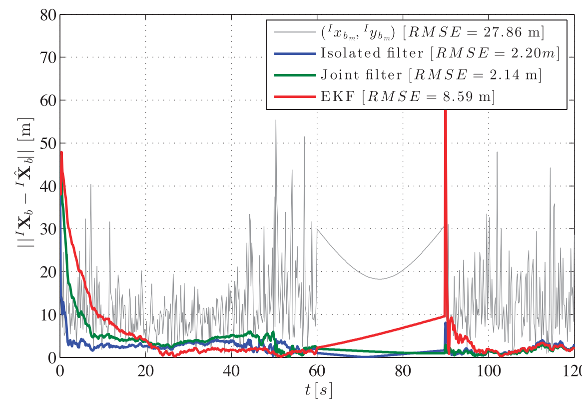

Fig. 11. Euclidean norm of estimation error of marine mammal's position when mammal moves with angular speed of third model and there are occlusions. Values in brackets are steady-state RMSEs of position estimates provided by each strategy.

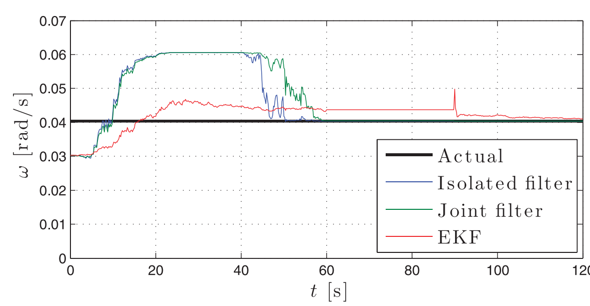

Fig. 12. Evolution over time of estimates for angular speed of marine mammal when actual angular-speed value is 0.04 rad/s and there are occlusions.

similar to their performance when there are no occlusions. This occurs because the model of the target has already been correctly identified, in both situations, by the time the marine mammal submerges (see Fig. 12). If this were not the case, a larger degradation in the performance of the filters would be observed. Such degradation is visible in the performance of the EKF (see Fig. 11), since the error in the estimates provided by this filter for the angular speed of the marine mammal is still significant at the time the mammal submerges (see Fig. 12). Using an inaccurate estimate for the angular speed during the 30 s of occlusion leads to the degradation of the quality of the position estimates.

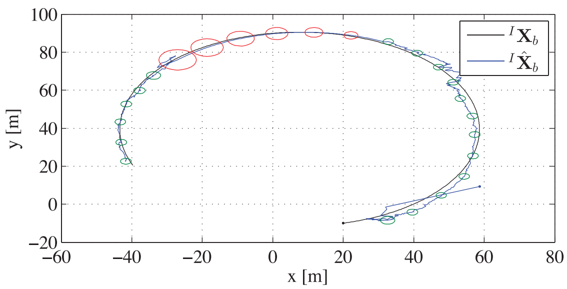

(a) Isolated MMAE.

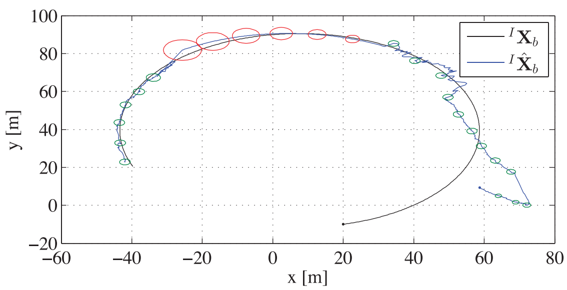

(b) Joint MMAE.

Fig. 13. Evolution of covariance of target position estimation error when there are occlusions and mammal moves with angular speed of third model. Green and red ellipses correspond to moments when target is visible by camera and submerged, respectively.

Even though the performance of the isolated and joint MMAEs does not degrade significantly during the occlusion of the marine mammal, the covariance of the error in the position estimates increases. This behavior was expected, since the update step is not performed during the interval in which the target is submerged, and can be confirmed by comparing the green and red ellipses in Fig. 13. In this figure, the ellipses represent the covariance of the target position estimation error. Their two semiaxes have direction and length given, respectively, by the eigenvectors and square root of the eigenvalues of the covariance matrices associated with the errors in the estimation of the position of the target.

V. CONCLUSIONS

This paper proposed new strategies to address the positioning and tracking problem of a target that moves at the sea surface and is recorded by a camera installed on a UAV that is equipped with a GPS receiver and an AHRS. Measurements of the centroid of the image of the target, which can be computed using active contours, were combined with the measurements provided by the GPS receiver and AHRS to obtain estimates of the position of the target with respect to an inertial reference frame. With this purpose, two Kalman filters were proposed: one, time invariant, that estimates only the position of the target, and the other, time varying, that improves the accuracy of the results by merging the estimates of the position of the target with estimates of the position of the UAV. To assess the performance of these approaches, a set of simulations, carried out under realistic conditions, were presented. Results obtained with a standard method based on the use of an EKF were also provided and compared with those obtained with the proposed strategies. Even though the three approaches had similar performances, the time-varying Kalman filter was the one that led to the best results for the presented experiments.

REFERENCES

[1] Zeller, D. C.
Ultrasonic telemetry: Its application to coral reef fisheries.
Fisheries Bulletin, **97**, 4 (1999), 1058–1065.

[2] Block, B. A., Dewar, H., Blackwell, S. B., Williams, T. D., Prince, E. D., Farwell, C. J., Boustany, A., Teo, S. L. H., Seitz, A., Walli, A., and Fudge, D.
Migratory movements, depth preferences, and thermal biology of Atlantic bluefin tuna.
Science, **293**, 5533 (17 Aug. 2001), 1310–1314.

[3] Sibert, J. R., and Nielsen, J. L. (Eds.)
Electronic Tagging and Tracking in Marine Fisheries.
Dordrecht, the Netherlands: Springer, 2001.

[4] Rosa, P., Silvestre, C., Cabecinhas, D., and Cunha, R.
Autolanding controller for a fixed wing unmanned air vehicle.
In *AIAA Guidance, Navigation and Control Conference and Exhibit*, Hilton Head, SC, Aug. 2007.

[5] Giraudet, P., and Glotin, H.
Real-time 3D tracking of whales by echo-robust precise TDOA estimates with a widely-spaced hydrophone array.
Applied Acoustics, **67**, 11–12 (2006), 1106–1117.

[6] Fekri, S., Athans, M., and Pascoal, A.
Issues, progress and new results in robust adaptive control.
International Journal of Adaptive Control and Signal Processing, **20**, 10 (2006), 519–579.

[7] Magill, D.
Optimal adaptive estimation of sampled stochastic processes.
IEEE Transactions on Automatic Control, **10**, 4 (Oct. 1965), 434–439.

[8] Gaspar, T., Oliveira, P., and Silvestre, C.
UAV-based marine mammals positioning and tracking system.
In *2011 International Conference on Mechatronics and Automation*, Beijing, China, Aug. 2011, 1050–1055.

[9] Kwon, H., Yoder, J., Baek, S., Gruber, S., and Pack, D.
Maximizing water surface target localization accuracy under sunlight reflection with an autonomous unmanned aerial vehicle.
Journal of Intelligent & Robotic Systems, **74**, 1 (Apr. 2014), 395–411.

[10] Choi, H., and Kim, Y.
Vision-based UAV guidance and estimation for aerial target tracking.
In *28th Congress of the International Council of the Aeronautical Sciences*, Brisbane, Australia, Sept. 2012.

[11] Han, K. M., and DeSouza, G. N.
Geolocation of multiple targets from airborne video without terrain data.
Journal of Intelligent & Robotic Systems, **62**, 1 (Apr. 2011), 159–183.

[12] Pirshayan, A., Seyedarabi, H., and Haghipour, S.
Target localization using cooperative unmanned aerial vehicles.
Advances in Computer Science: An International Journal, **3**, 4 (July 2014), 68–73.

[13] Selby, W., Corke, P., and Rus, D.
Autonomous aerial navigation and tracking of marine animals.
In *Proceedings of Australasian Conference on Robotics and Automation*, Melbourne, Australia, Dec. 2011.

[14] Kaiser, M. K., Gans, N. R., and Dixon, W. E.

Vision-based estimation for guidance, navigation, and control of an aerial vehicle.
IEEE Transactions on Aerospace and Electronic Systems, **46**, 3 (July 2010), 1064–1077.

[15] Zhang, J., Wu, Y., Liu, W., and Chen, X.
Novel approach to position and orientation estimation in vision-based UAV navigation.
IEEE Transactions on Aerospace and Electronic Systems, **46**, 2 (Apr. 2010), 687–700.

[16] Sohn, S., Lee, B., Kim, J., and Kee, C.
Vision-based real-time target localization for single-antenna GPS-guided UAV.
IEEE Transactions on Aerospace and Electronic Systems, **44**, 4 (Oct. 2008), 1391–1401.

[17] Wang, I. H., Dobrokhodov, V. N., Kaminer, I. I., and Jones, K. D.
On vision-based target tracking and range estimation for small UAVs.
In *AIAA Guidance, Navigation and Control Conference and Exhibit*, San Francisco, CA, Aug. 2005.

[18] Dobrokhodov, V. N., Kaminer, I. I., Jones, K. D., and Ghabcheloo, R.
Vision-based tracking and motion estimation for moving targets using small UAVs.
In *2006 American Control Conference*, Minneapolis, MN, June 2006.

[19] Rysdyk, R.
UAV path following for constant line-of-sight.
In *2nd AIAA "Unmanned Unlimited" Systems, Technologies and Operations—Aerospace, Land and Sea Conference*, San Diego, CA, Sept. 2003.

[20] Heintz, F., Rudol, P., and Doherty, P.
From images to traffic behavior—A UAV tracking and monitoring application.
In *10th International Conference on Information Fusion*, Quebec, Canada, July 2007.

[21] He, R., Prentice, S., and Roy, N.
Planning in information space for a quadrotor helicopter in a GPS-denied environment.
In *IEEE International Conference on Robotics and Automation*, Pasadena, CA, May 2008, 1814–1820.

[22] Patterson, T. A., Thomas, L., Wilcox, C., Ovaskainen, O., and Matthiopoulos, J.
State–space models of individual animal movement.
Trends in Ecology & Evolution, **23**, 2 (Feb. 2008), 87–94.

[23] Li, X. R., and Jilkov, V. P.
Survey of maneuvering target tracking.
Part I: Dynamic models. IEEE Transactions on Aerospace and Electronic Systems, **39**, 4 (Oct. 2003), 1333–1364.

[24] Rugh, W. J.
Linear System Theory (2nd ed.). Upper Saddle River, NJ: Prentice Hall, 1996.

[25] Faugeras, O., and Luong, Q.-T.
The Geometry of Multiple Images. Cambridge, MA: MIT Press, 2001.

[26] Kass, M., Witkin, A., and Terzopoulos, D.
Snakes: Active contour models.
International Journal of Computer Vision, **1**, 4 (Jan. 1988), 321–331.

[27] Leymarie, F., and Levine, M. D.
Tracking deformable objects in the plane using an active contour model.
IEEE Transactions on Pattern Analysis and Machine Intelligence, **15**, 6 (June 1993), 617–634.

[28] Baram, Y.
Information, consistent estimation and dynamic system identification.
Ph.D. dissertation, Massachusetts Institute of Technology, Cambridge, 1976.

[29] Murray, R. M., Li, Z., and Sastry, S. S.
A Mathematical Introduction to Robotic Manipulation. Boca Raton, FL: CRC Press, 1994.

[30] Gelb, A. (Ed.)
Applied Optimal Estimation. Cambridge, MA: MIT Press, 1974.

[31] Anderson, B. D. O., and Moore, J. B.
Optimal Filtering. Englewood Cliffs, NJ: Prentice-Hall, 1979.

[32] Simanek, J., Reinstein, M., and Kubelka, V.
Evaluation of the EKF-based estimation architectures for data fusion in mobile robots.
IEEE/ASME Transactions on Mechatronics, **20**, 2 (Apr. 2015), 985–990.

[33] Chen, S. Y.
Kalman filter for robot vision: A survey.
IEEE Transactions on Industrial Electronics, **59**, 11 (Nov. 2012), 4409–4420.

[34] Brás, S., Cunha, R., Vasconcelos, J. F., Silvestre, C., and Oliveira, P.
A nonlinear attitude observer based on active vision and inertial measurements.
IEEE Transactions on Robotics, **27**, 4 (Aug. 2011), 664–677.

Tiago Gaspar received an M.Sc. degree in electrical and computer engineering in 2008 from the Instituto Superior Técnico, Lisbon, Portugal, where he is currently pursuing a Ph.D. degree in the same field. His research interests include positioning and tracking systems, sensor and signal fusion, nonlinear estimation, and video synchronization.

Paulo Oliveira received a Ph.D. degree in electrical and computer engineering from the Instituto Superior Técnico (IST), Lisbon, Portugal, in 2002. He is an associate professor in the department of mechanical engineering at IST and a researcher in the Institute of Mechanical Engineering, IST. He also collaborates with the Institute for Systems and Robotics, IST. His areas of scientific activity are mechatronics with special focus on the fields of autonomous vehicles, robotics, sensor fusion, navigation, positioning, and nonlinear estimation. Over the last 25 years he has participated in more than 30 European and Portuguese research projects and coauthored more than 50 journal and 150 conference papers.

Carlos Silvestre received a Licenciatura degree in electrical engineering from the Instituto Superior Técnico (IST), Lisbon, Portugal, in 1987 and an M.Sc. degree in electrical engineering and a Ph.D. degree in control science from the same school in 1991 and 2000, respectively. In 2011 he received a Habilitation in electrical engineering and computers also from IST. Since 2000 he has been with the department of electrical engineering at the Instituto Superior Técnico, where he is currently an associate professor of control and robotics on leave. Since 2015 he has been a professor in the department of electrical and computers engineering of the Faculty of Science and Technology at the University of Macau. Over the past years, he has conducted research in the subjects of navigation, guidance, and control of air and underwater robots. His research interests include linear and nonlinear control theory, coordinated control of multiple vehicles, gain-scheduled control, integrated design of guidance and control systems, inertial navigation systems, and mission control and real-time architectures for complex autonomous systems with applications to unmanned air and underwater vehicles.